Powder Technology 367 (2020) 671–679

Contents lists available at ScienceDirect

Powder Technology

journal homepage: www.elsevier.com/locate/powtec

Review

A simple method for assessing powder spreadability for additive manufacturing

Moustafa Ahmed [a], Mehrdad Pasha [a], Wenguang Nan [a,b], Mojtaba Ghadiri [a,*]

[a] School of chemical and process Engineering, University of Leeds, Leeds LS2 9JT, UK
[b] School of Mechanical and Power Engineering, Nanjing Tech University, Nanjing 211816, China

ARTICLE INFO

Article history:
Received 21 January 2020
Received in revised form 7 April 2020
Accepted 10 April 2020
Available online 11 April 2020

Keywords:
Powder spreading
Spreadability
Additive manufacturing
Empty patches
Jamming
Feedstock

ABSTRACT

Additive manufacturing based on powder spreading is attracting great interest, but one key weakness is that narrow gaps used for spreading produce non-uniformity in the spread layer due to transient jamming. We propose a simple technique for assessing the powder spreadability, a measure of the ease with which a powder is spread uniformly without the formation of empty patches. A cutter blade, with a segment cut along its length to produce a gap, is used to manually spread a small heap of powder. The frequency of formation of empty patches and their size, which are a manifestation of jamming as the particles are spread, are analysed for several gap heights. The sizes of the empty patches and frequency of their formation are determined by image analysis. The outcomes correlate well with a Discrete Element Method simulation of the same system. A criterion is proposed for diagnosing the empty patch formation.

Contents

1. Introduction

Additive manufacturing (AM) is going through exponential growth in various industries such as medical, aerospace, construction and biology [1–5]. The inherent ability of AM to produce complex and personalised three-dimensional objects from Computer Aided Designs (CAD) using layer upon layer approach has attracted great attention [1], as it side-lines the necessity of expensive and time-consuming tooling of conventional manufacturing methods for producing the same objects [2,3,5]. Broadly, AM could be classified into two manufacturing techniques, powder-based process and liquid-based feed process [4,5]. Here we address the former, where the powder is spread over a particle bed as a thin layer by a roller or blade to the thickness of a few particle diameters [6,7]. Laser or electron beams are shone on to the layer in a scanning mode to melt/sinter a selected area. Afterwards, the particle bed is then lowered and the process is repeated until production is finished [6,7]. The powder particles size and shape are critical factors, as the particles should be small enough for rapid sintering and melting when an energy beam is applied, but at the same time sufficiently free-flowing to avoid inconsistent flow and sensitivity to operation speed [8,9]. Spreading powders by a blade or roller

---

[*] Corresponding author.
E-mail address: m.ghadiri@leeds.ac.uk (M. Ghadiri).

https://doi.org/10.1016/j.powtec.2020.04.033
0032-5910/

with very small gaps may cause problems, such as mechanical arching and transient jamming [10], posing a major manufacturing bottleneck, as it impacts on the quality and characteristics of the final product and also on the production speed. Patchy coverage produces defects in the product by adversely affecting particle bonding in the sintering/melting process, and ultimately resulting in lower quality product [11,12]. Addressing the issues through heuristic methods is expensive and flaws can only be detected after the specimen is made [11,12]. Therefore an in-depth understanding of cohesive and frictional powder flows in narrow spreading gaps is helpful for further development of this technology and introduction of new materials. Currently, there are three techniques for investigating powder spreadability for AM, experimental, numerical simulation by the Discrete Element Method (DEM) and Machine Learning (ML) [13]. By spreadability we mean the complex characteristic features of a powder (as obviously influenced by particle properties), which allow the powder to be spread uniformly as a thin layer of a few multiples of particle size without the formation of any empty patches, presence of agglomerates and rough surfaces.

The majority of the studies conducted so far address powder flowability instead of spreadability [14–26] using various characterisation techniques and devices for bulk cohesive powder flow [27]. Even in this situation the number of devices available for rheological characterisation of powders in a wide range of shear strain rates is limited to Anton-Paar Powder Cell, Couette device, FT4 Powder Rheometer, ball indentation method and rotating drum. In any case, the above mentioned methods and instruments are good for assessing the flowability of cohesive powders under dynamic conditions, but spreadability and flowability are two different measures of powder bulk flow characteristics, albeit inter-related. The former, which is the focus of the work here, is affected by powder flow behaviour in narrow clearances, where the shearing zone is only a few multiple of particle size, thus the discrete nature and properties of particles, such as size distribution, shape and surface properties are highly influential in transient jamming over the clearance. In a recent study, Snow et al. [28] point out the need for developing spreadability metrics. They attempted to establish a powder spreadability metrics by comparing powder spreading pattern (the fraction of powder coverage of the build plate) with results from analysis of the rate of powder deposition, the average avalanching angle of the powder heap, and the rate of change of the avalanching angle. They report the average avalanching angle does not provide a good correlation with the angle of repose, whilst the other metrics do. However, the angle of repose is not a clear indicator of either flowability or spreadability. Therefore, a criterion needs yet to be developed for describing the powder spreadability. Although various DEM simulation works have been done on the powder spreading [10,29–34], there is no experimental technique so far to assess powder spreadability.

Hence, in this work we use a model metal powder commonly used for additive manufacturing and propose a simple and quick experimental technique for characterising its spreadability as a function of the spreading gap height. The analysis is performed on the same metal powder as previously characterised for particle shape, interfacial adhesion and friction and used in the simulations by DEM [10]. A laser cut Stanton cutter blade of various gap heights positioned vertically is used to manually spread a pile of powder particles on frictional Emery paper to produce a spread layer. The generated particle spread layer contains empty patches (manifestation of jamming). The characteristics of empty patches in terms of size and frequency of appearance is analysed, providing a quick and simple method for characterising the spreadability of metal powders. The results are compared with numerical simulations by DEM.

2. Materials and method

2.1. Materials

The test powder is gas-atomised 316 L stainless steel particles, obtained from Sandvik Osprey Ltd., Neath, UK. Its particle size distribution is in the range 15–55 μm, with the characteristic measures of the distribution D_{10}, D_{50} and D_{90} by number given as 20 μm, 32 μm and 45 μm, respectively. Nan et al. [10] have shown that the most appropriate characteristic measure of particle size that describes transient jamming and powder flow through narrow gaps is D_{90} by number (will be denoted as D in this work). As we use the same powder in our work, the relevant particle properties are those reported by Nan et al. [10]. The particle size distribution is classified into four sizes classes as reproduced here as Fig. 1.

A Stanton cutter blade is used for powder spreading. It is cut along its length by laser to create a gap in the middle as shown in Fig. 2. Blades with five depths of cut are prepared, i.e. 45 μm, 67.5 μm, 90 μm, 112.5 μm and 135 μm, corresponding to multiples of D to enable powder spreading with different gap heights. SEM images of all the blades were analysed to measure the actual gap height for every blade. They were all close to the nominal values with a tolerance of ±0.2 μm.

To provide a fully-rough base, several abrasive Emery papers with different levels of fineness were assessed. Among them, the CarbiMet PSA, 1000 [P2500] gives the most uniform spreading, and it is used in this work. It is made of silicon carbide and has a grit designation of 1000 [P2500], with an average particle diameter of 10.3 μm [35]. A SEM image of the rough base is presented in Fig. 3.

2.2. Methodology

To provide an appropriate amount of powder for spreading, a makeshift cardboard stencil (25 mm × 2.5 mm) was made to deliver a consistent amount of powder for every spreading experiment, shown as a CAD model in Fig. 4(a). The Emery paper is cut to the size of a standard microscope glass slide (75 mm × 25 mm), and is glued to the glass slide (i.e. the right slide in Fig. 4(b)) with a thin glue and compressed by dead-weight to ensure flatness. The glass slide is placed next to another glass slide (i.e. the left slide in Fig. 4(b)), to provide a flat surface to place the cardboard stencil on top of them so that it does not tilt. The powder is poured over the slot of the stencil until it is full, and the excess powder is scrapped off using a blade, as shown in Fig. 4(c)–(d). The cardboard stencil is then removed carefully, producing a heap of powder, as shown in Fig. 4(e). The support glass slide (i.e. the left one in Fig. 4 (b)) is removed and a spread blade with a known gap height is swiped manually over the heap to spread the powder in the direction indicated by the arrow in Fig. 4(f). Powder spreading is video-recorded at 240

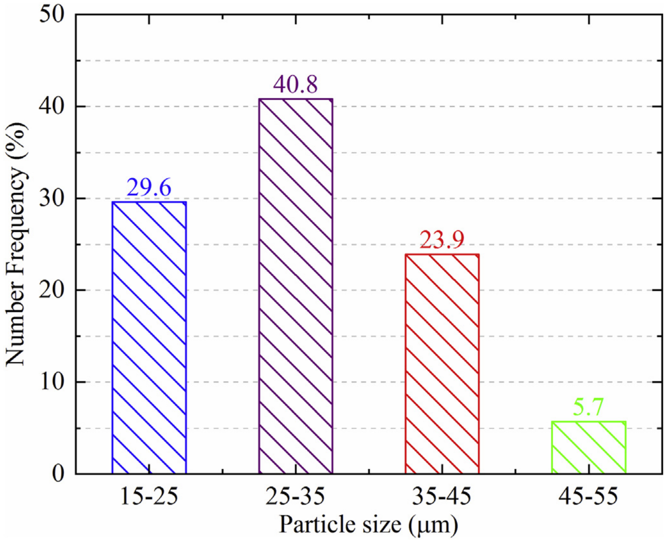

Fig. 1. Particle project-area equivalent-circle diameter distribution by number of Sandvik powder classified in four size classes, with D_{10}, D_{50} and D_{90} of the number distribution given as 20 μm, 32 μm and 45 μm, respectively [10].

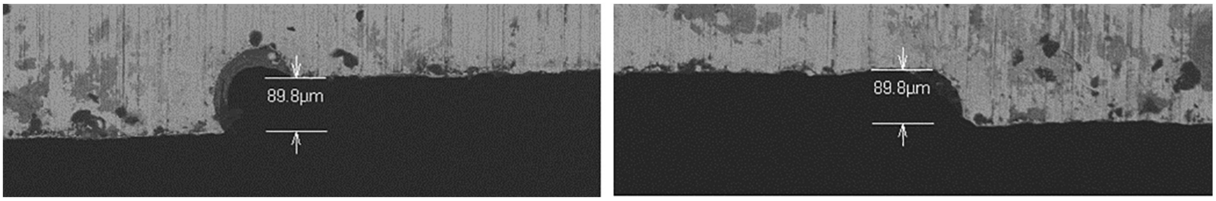

Fig. 2. SEM images of the left and right sides of a Stanton cutter blade, cut along its length by laser to create a gap in the middle, in this case a gap height of 90 µm.

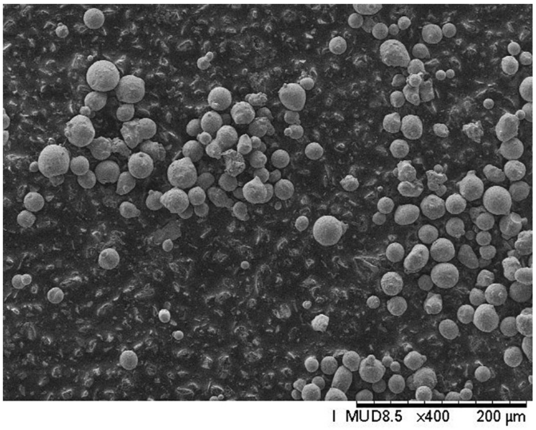

Fig. 3. SEM image of the rough base (i.e. Emery paper) with partially covered metal particles.

frames per second (FPS). Following the spreading process, the particles are immobilised by using an adhesive spray to enable the handling of the spread layer for SEM analysis. Finally, the aforementioned steps are repeated three times for each gap height, and their respective recording of each spreading process is transferred to PC for analysis.

2.2.1. Spread uniformity

The quality of the spread layer in terms of the presence of empty patches is determined by image analysis. For this purpose, a Hitachi TM3030Plus SEM is used at 150× magnification, backscattered mode and 15 kV. A series of images are taken in the spreading direction, as shown in Fig. 5. The images are collated to form a composite image of the entire length of spread layer, as shown by the rectangle in Fig. 5 (c). This provides an image with good depth of field and appropriate resolution.

The SEM images are first analysed by ImageJ software for pre-processing [36], and then passed to MATLAB R2018a for further analysis of empty patches. The images are set at 1.2 µm/pixel scale, and

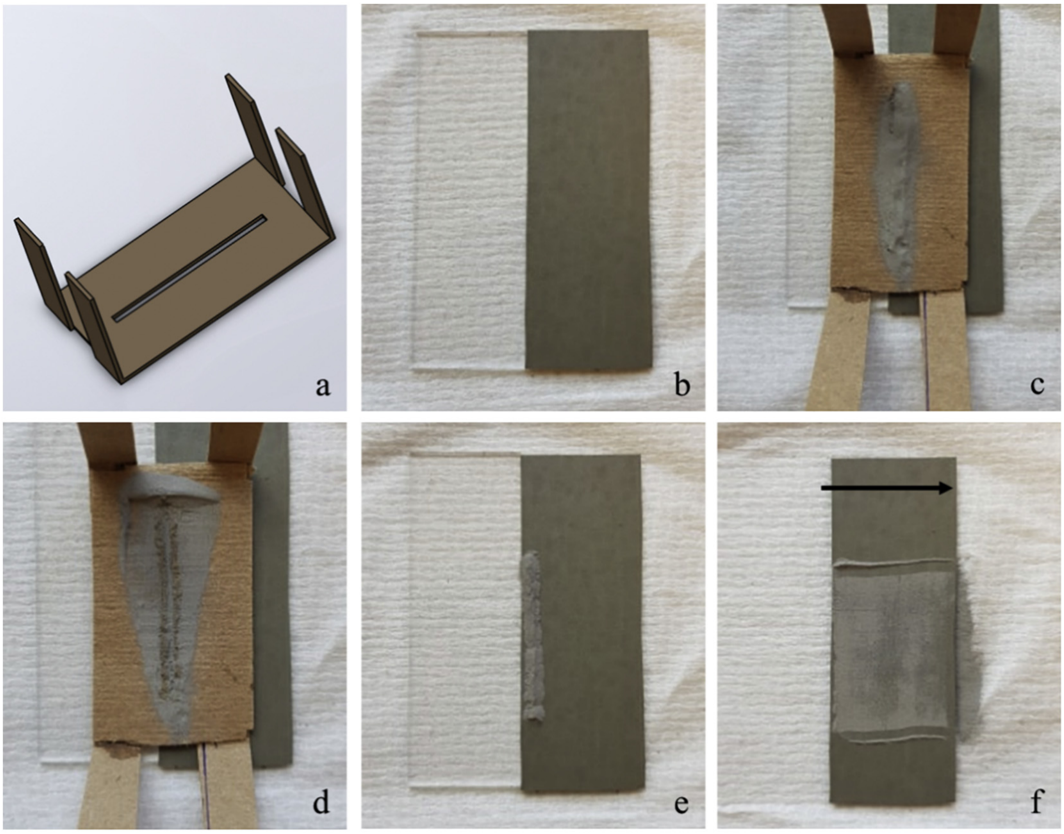

Fig. 4. Summary of the experimental procedure: (a) makeshift cardboard stencil (25 mm × 2.5 mm), (b) a glass slide (the right slide) covered by Emery paper with another glass slide (the left one) placed next to it; (c) powder is poured over the slot of the stencil; (d) excess powder is scrapped off; (e) cardboard stencil is removed to produce a heap of powder; (f) a spread blade is swiped manually over the heap after removing the support glass slide (the left one).

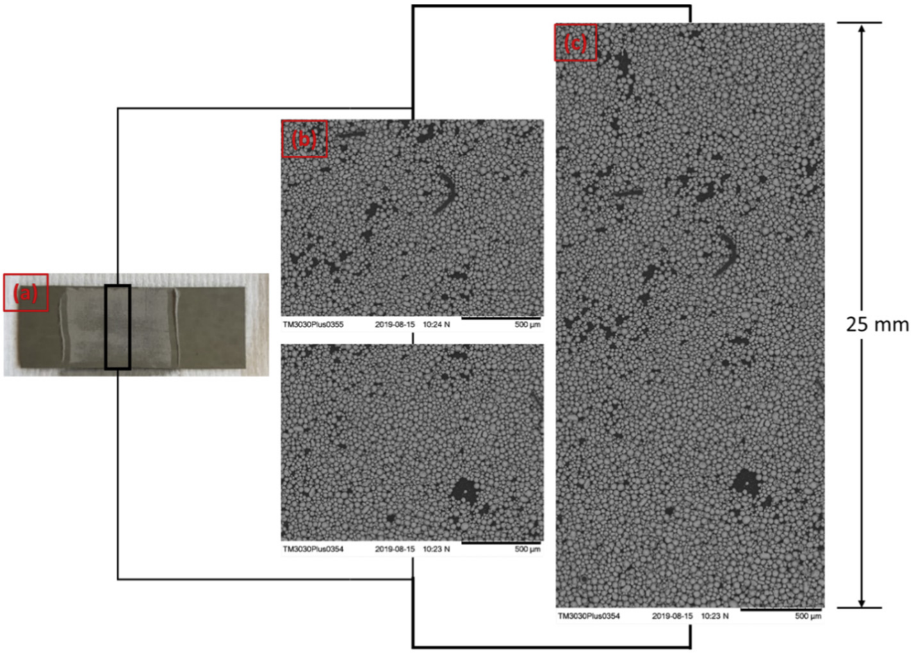

Fig. 5. (a) A photo of the powder layer, (b) SEM images of segments of the layer, and (c) the collection of segmented images showing the spread bound by the rectangle seen in (a).

converted to a 16-bit image. Denoising plugin feature is used to add clarity to the SEM images post-filtering [37]. Two threshold images are applied via default auto-threshold methods, one for the voids and one for the particles to ease analysis in the following steps, as shown in Fig. 6. The size analysis is initiated and the two images are passed to MATLAB R2018a for analysis. The image of particles is first dilated by five pixels (established by trial-and-error). This is done to filter out the noise in the image analysis process brought by the small empty patches/areas, and they are also of no interest, as they do not constitute empty patches, due to their extreme small sizes (<6 μm), and to define specific perimeters of empty patches, as the interest is in their size and number density. An eroded image of the voids is created by subtracting the newly-created dilated particles image from the original binary voids image which is 'thresholded'. The voids in the newly-eroded image are dilated to regain their original size, while also having definite perimeters of empty patches of interest. Small objects (such as the small voids between the particles) in the newly-formed image are removed, since the interest is in the voids of certain size and number density. The desired parameters (length, area and location of the empty patches) are determined as described in the following section.

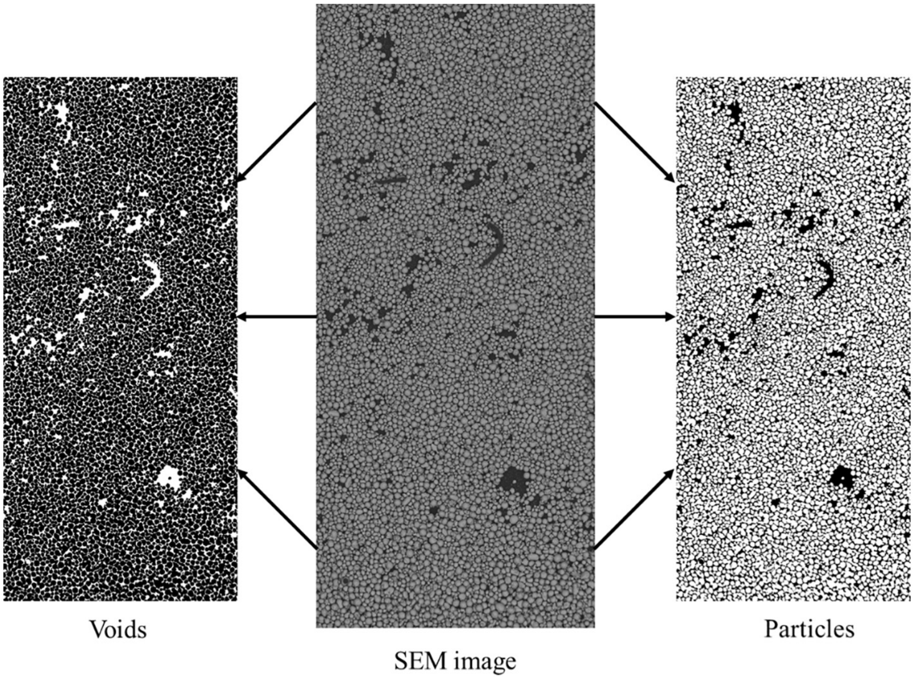

Fig. 6. *Thresholding of SEM images for analysis*, where two thresholding actions are applied via default auto-threshold methods, one for the voids and one for the particles.

2.2.2. Determination of the spreader speed

The recordings of the spread, taken at 240 frames per second (fps), were transferred to a computer for analysis. A separate MATLAB code was used to extract each individual frame from all the recordings. The frames that captured the spreading process were counted, and the time taken for the spread was ascertained from the FPS and the average spreading speed was hence calculated from the spreading distance (25 mm) and time, as described later below.

3. Results and discussion

The experiments were repeated three times to check for reproducibility for each of the individual gap height. The gap heights were actually 1, 1.5, 2, 2.5 and 3 multiples of D_{90}, respectively, as the work of Nan et al. [10] had previously shown that D_{90} of the particle size distribution by number was accountable for transient jamming, and hence the quality of spreading. The results of the three repeats are denoted as R1, R2 and R3, respectively. However for brevity only the results of R1 is reported here, but all the three repeats are used in the analysis. The SEM images of R1 for the five gap heights are shown in Fig. 7 (these images are actually magnifiable to high resolution 1.2 μm/pixel). It can easily be observed by naked eye that the frequency of empty patches decreases sharply with increasing gap height. The SEM images were processed by ImageJ to create two threshold images of each gap height. The compilation of the threshold images of both voids and particles is shown in Fig. 8 for the smallest gap height, i.e. D_{90}, showing the empty patches. The pattern of empty patches is similar to the simulation results of the spreading of the same powder layer reported by Nan et al. [10] based on visual observations. This is shown in Fig. 9 for the simulation work along with the experimental results obtained here.

The threshold images are analysed quantitatively by MATLAB to calculate the length, area and location of each empty patch, i.e. its respective x and y coordinates. Following this step the time of spreading is determined for the evaluation of the frequency of formation of empty patches. The spreading time and average speed are calculated by MATLAB for R1 and are given in Table 1.

As the time for each spread and the number and length of empty patches are determined, their frequency of occurrence could be calculated in the same way as done by Nan et al. [10], i.e. by dividing the number of empty patches by the spreading time for each gap height. However, to fit the scale necessary to compare the results with those of Nan et al. [10] (see the patch length/D cells in Table 2), each individual length is divided by D (i.e. 45 μm), so as to present it as a multiple of D (normalised length).

The frequency of formation of empty patches of different lengths can now be calculated using both time for each individual length scale and the number of empty patches. For brevity, only the frequency and the empty patch length results of R1 are shown in Fig. 10 for all the gap heights tested.

There is a significant decrease in the frequency of empty patches with increasing empty patch length. This is correlated with the jamming events of particle flow in the gap region. The jamming events with shorter survival times produce smaller empty patches, and have a much larger occurrence frequency [10]. Additionally, with increasing gap height, it is apparent that the frequency decreases rapidly and for increased empty patch lengths, the frequency is mainly composed of small gap heights (i.e. the spread layer is more uniform with large gap heights). The simulation predictions of Nan et al. [10] for exactly the same system is reproduced as Fig. 11 for comparison, where a good correlation is observed.

Furthermore, both Figs. 10 and 11 exhibit a puzzling occurrence of a sudden increase in frequency of empty patches (gap height *2.5D* for *(2–3)/D* in Figs. 10 and *1.75D* for *(2–3)/D* in Fig. 11). As three repeats have been carried out for each gap height, and the results combined, the consistent trend here requires further systematic analysis.

To compare the probability of the formation of empty patches of all sizes with those of the simulation results, the sum of the number of all the empty patches (regardless of their size range) is calculated for the same gap height. For example, from Table 2 for gap height 1, the total number of relevant empty patches is the sum of 303, 45, 13, 5, 19, i.e. 385. Therefore, the probability of the formation of the empty patches for the size class 2–3 is 303/385, i.e. 0.78. As the probability of formation of the empty patches is established, a plot of the probability versus the length of empty patches is plotted as shown in Fig. 12 for R1 and then compared to the simulation results in Fig. 13 reported by Nan et al. [10].

As it could be seen from Figs. 12 and 13, with increasing patch lengths, the probability of formation of longer patches decreases. Additionally, for the smallest patch lengths (2–3), it could be concluded that it is almost certain that all the empty patches generated by large gap heights (3 and 2) fall within this size criterion, while it becomes less frequent with greater patch lengths and roughly non-present in the greatest size range (≥10). This indicates that large gap heights (above *(2–3)/D*) give a more uniform spread layer without the formation of empty patches, due to less jamming, as intuitively expected. So spreadability can be defined based on a criterion for empty patch formation, considering the largest patch size which is acceptable for spreading and its formation frequency. This is obviously correlated with frequency and period of transient jamming. The location of the empty patches is predicted based on its size following the approach of Nan et al. [10]. The particle layer is divided into bins of size $\Delta y = 1.25D$ and $\Delta x = 2D$ in the y and x directions, respectively. The location

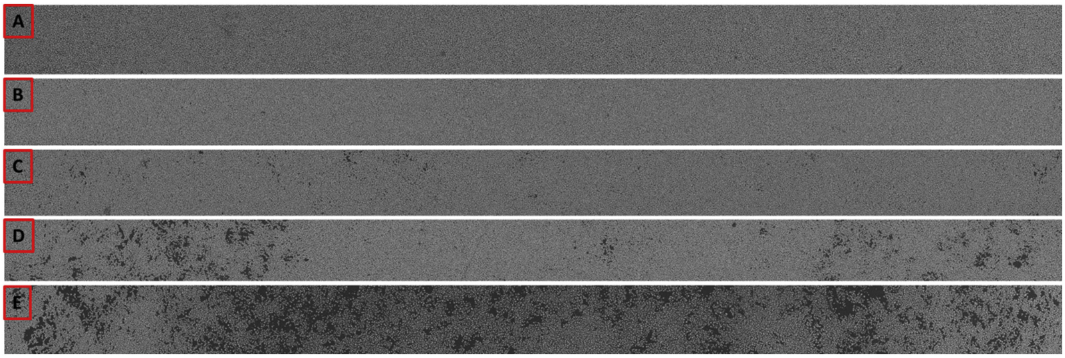

Fig. 7. Compilation of the SEM images of R1, where A, B, C, D and E refer to the gap heights 3, 2.5, 2, 1.5 and 1 multiples of D_{90}, respectively. These images are actually magnifiable to high resolution 1.2 μm/pixel.

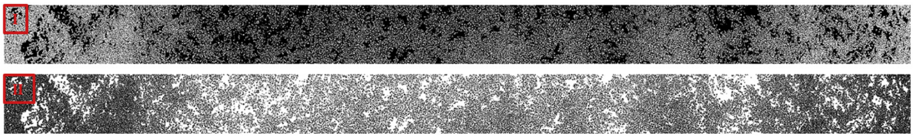

Fig. 8. Threshold images of the smallest gap height, i.e. D_{90} of R1, where I and II refer to the threshold images of the particles and voids, respectively.

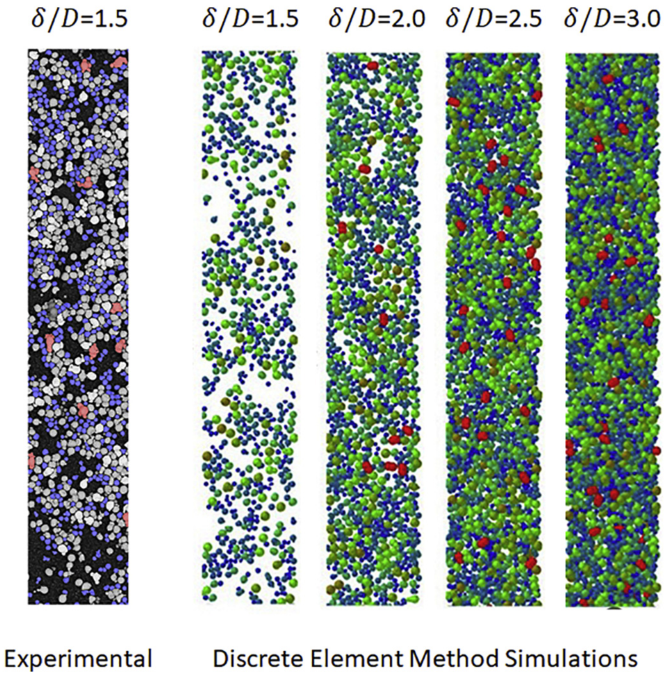

Fig. 9. DEM simulation and experimental spread of gas-atomised metal powder via a blade [27], where a similar pattern of empty patches is observed in both works.

Table 1
Summary of the spreading time and average speed of R1.

Gap height/D	Number of frames	Time (s)	Average Speed (m/s)
1.0	595	2.48	0.010
1.5	484	2.02	0.012
2.0	566	2.36	0.010
2.5	484	2.02	0.009
3.0	561	2.34	0.010

Table 2
Number of empty patches for each patch length range for R1.

Gap height/D	1.0	1.5	2.0	2.5	3.0
Patch length/D	Number of empty patches				
2–3	303	167	95	120	58
4–5	45	23	7	16	1
6–7	13	7	3	3	0
8–9	5	4	1	0	0
≥10	19	12	0	0	0
Time (s)	2.48	2.02	2.36	2.02	2.34

of each empty patch is estimated based on its size. So if the particle fraction in the bin falls below a critical value, the bin is designated as empty. The following criterion (eq. 1) was proposed by Nan et al. [10] based on trial and error.

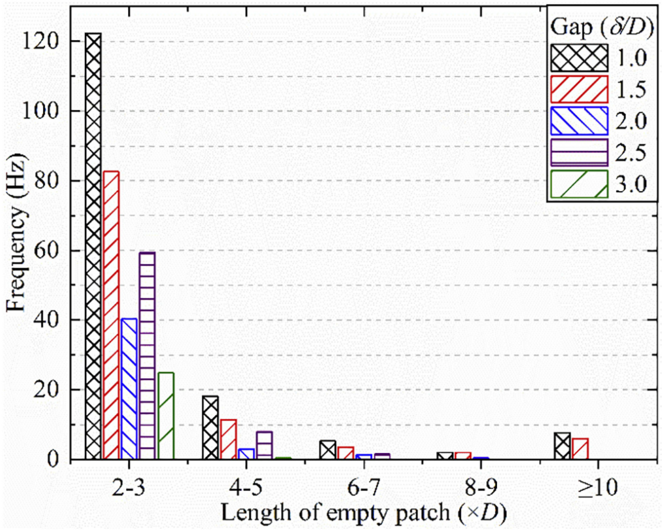

Fig. 10. Frequency of formation of empty patches of various length for R1, where the frequency of empty patches decreases significantly with increasing empty patch length.

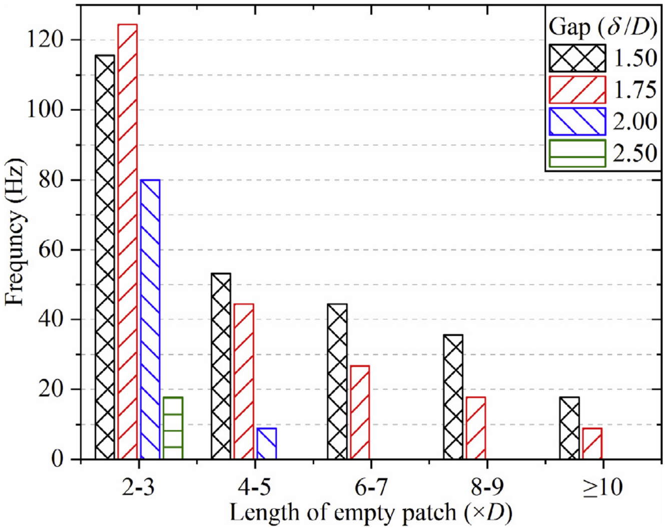

Fig. 11. Simulation predictions of frequency of jamming as a function of empty patch length [10].

$$\frac{\sum V_p}{\Delta x \times \Delta y \times (\delta - \delta_c)} < 0.1 \qquad (1)$$

where V_p is the particle volume, and δ_c is the critical gap (1.0D). In practise it is difficult to account for volume measures from a 2-D image, hence the area of each particle (A_p) is considered instead. Therefore the volume criterion is modified to fit the particle area by considering that the analysed image is 2-D, the particle fraction becomes the

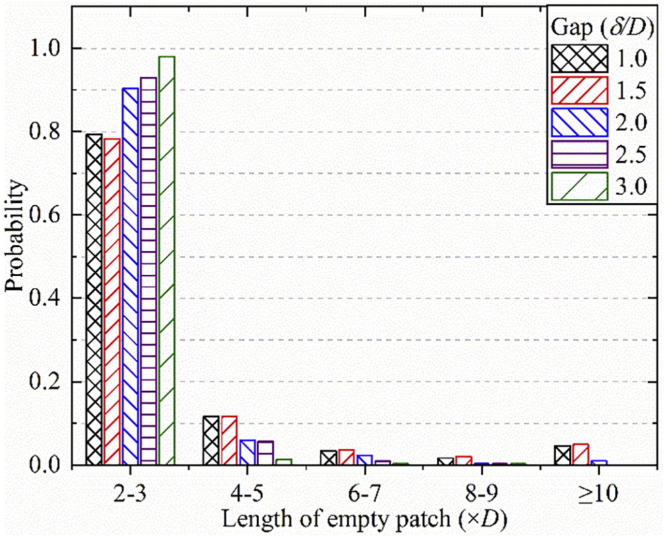

Fig. 12. A plot of probability against the length of empty patches for R1, where the probability of formation of longer patches decreases with increasing patch lengths.

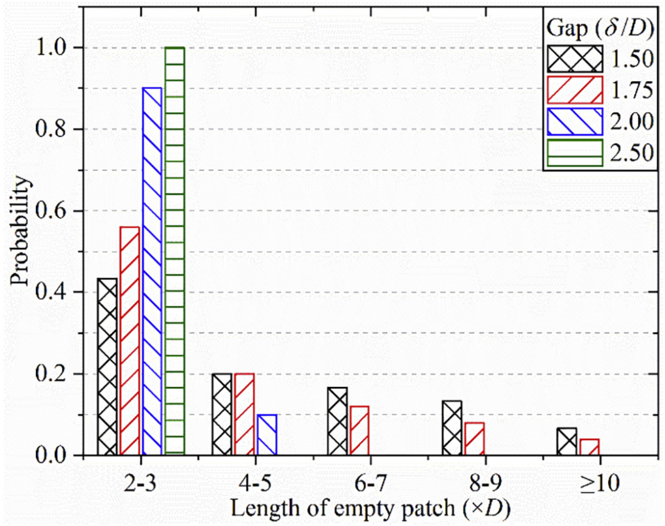

Fig. 13. The distribution of probability of the number of empty patches with each patch length [10].

number of particles in a given area (area of the bins) and thus the term ($\delta - \delta_c$) is neglected (see Fig. 14). Instead a 2-D criterion (eq. 2) is adopted by trial and error. It is found that the following criterion gives equivalent locations of empty patches.

$$\frac{\sum A_p}{\Delta x \times \Delta y} \leq 0.3 \tag{2}$$

The area of the particles is determined through MATLAB using the threshold image of the particles for each gap height as given previously in Fig. 8. Similar to Nan et al.'s work [10], an overlap of adjacent bins by 50% is considered to ensure that any of generated empty patches are of size $2D$ and greater. The locations of the empty patches for R1 are shown in Fig. 15, along with the simulation results in Fig. 16 reported by Nan et al. [10]

Similar to the trend observed by Nan et al. [10], Fig. 15, has legends/markers that indicate the location of empty patches present in their respective x/D values. The connected markers indicate that the legend/markers are related to the same empty patch. Additionally, with increased gap height, the number of empty patches decreases abruptly. Fig. 15 shows that for the gap height 3.0 there are no empty patches present, while for decreasing gap heights (1–2.5) the legends/markers that are indicative of empty patches are decreasing significantly. The experimental empty patches together with their indicator according to the criterion of eq. 2 are shown in Fig. 15, providing also a good correlation with the work of Nan et al. [10] shown as Fig. 16.

4. Conclusions

Spreadability of gas-atomised metal powders is assessed by a simple manual technique, utilising blades of various gap heights and an abrasive paper as a fully-rough frictional base. A heap of powder is placed on the base using a stencil and is swiped by a blade manually. The produced spread layer is then immobilised using an adhesive spray, and analysed using SEM and MATLAB to check the uniformity of the spread layer. The test is repeated for several blades of different gap heights. The spreadability of powder is quantified by the features of empty patches of the spread layer. Large empty patches are formed in small gap heights and are a manifestation of transient jamming of the powder in the heap around the gap. The frequency of formation of empty patches and their size are quantified by image analysis of scanning electron micrographs. They both decrease significantly with increasing gap height and vice versa. A criterion is proposed to identify an empty patch and predict its location along the spreading direction. In addition it is shown that the results are consistent with predictions by numerical simulations of the same powder system.

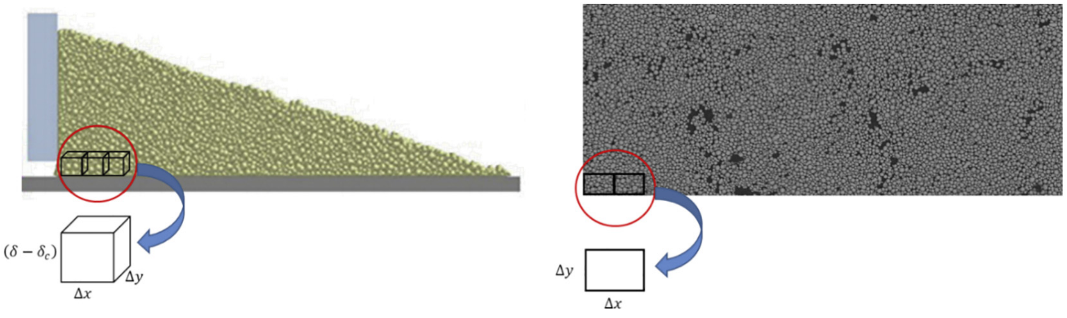

(a) (b)

Fig. 14. Different evaluation method for packing fraction: (a) based on volume fraction of Nan et al.'s work [10], (b) based on area in this work.

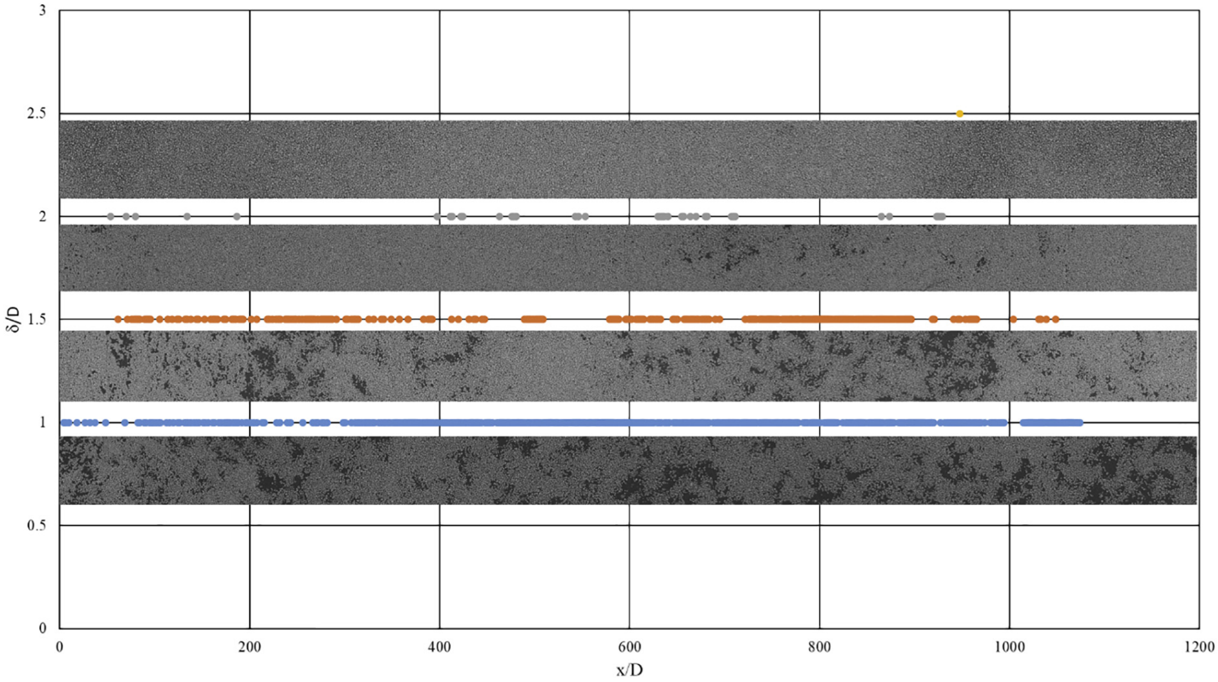

Fig. 15. Illustration of the location of the empty patches of R1 as identified by eq. (2) based on experimental results, where the legends/markers indicate the location of empty patches present in their respective x/D values, and the connected markers indicate that the legend/markers are related to the same empty patch.

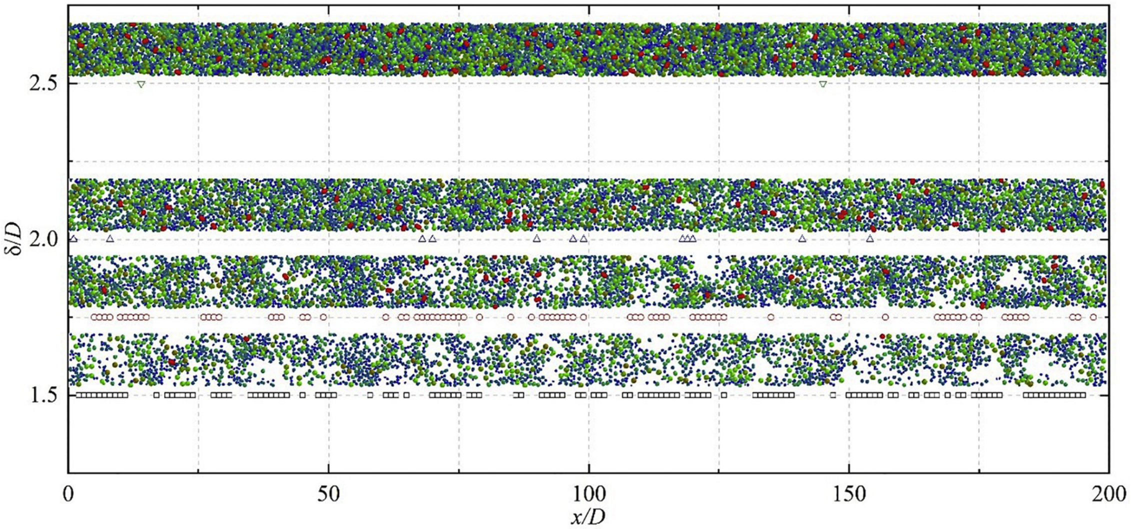

Fig. 16. Illustration of the location of empty patches as identified by simulation [10].

Acknowledgments

The support of the Virtual Formulation Laboratory Grant of the EPSRC Future Formulation Programme (EP/N025261/1) is gratefully acknowledged. The authors are grateful to Dr. Umair Zafar for his help during the initial stages of the work.

Declaration of Competing Interest

The authors declare that they have no known competing financial interests or personal relationships that could have appeared to influence the work reported in this paper.

References

[1] W.J. Sames, F.A. List, S. Pannala, R.R. Dehoff, S.S. Babu, The metallurgy and processing science of metal additive manufacturing, Int. Mater. Rev. 61 (2016) 315–360.

[2] T. Debroy, H.L. Wei, J.S. Zuback, T. Mukherjee, J.W. Elmer, J.O. Milewski, A.M. Beese, A. Wilson-Heid, A. De, W. Zhang, Additive manufacturing of metallic components – process, structure and properties, Prog. Mater. Sci. 92 (2018) 112–224.

[3] T.D. Ngo, A. Kashani, G. Imbalzano, K.T.Q. Nguyen, D. Hui, Additive manufacturing (3D printing): a review of materials, methods, applications and challenges, Compos. Part B 143 (2018) 172–196.

[4] K.V. Wong, A. Hernandez, A review of additive manufacturing, ISRN Mech. Eng. 2012 (2012) 10.

[5] S.A.M. Tofail, E.P. Koumoulos, A. Bandyopadhyay, S. Bose, L. O'Donoghue, C. Charitidis, Additive manufacturing: scientific and technological challenges, market uptake and opportunities, Mater. Today 21 (2018) 22–37.

[6] I. Yadroitsev, A. Gusarov, I. Yadroitsava, I. Smurov, Single track formation in selective laser melting of metal powders, J. Mater. Process. Technol. 210 (2010) 1624–1631.

[7] S.M. Thompson, L. Bian, N. Shamsaei, A. Yadollahi, An overview of direct laser deposition for additive manufacturing; part I: transport phenomena, modeling and diagnostics, Addit. Manuf. 8 (2015) 36–62.

[8] L.E.J. Thomas-Seale, J.C. Kirkman-Brown, M.M. Attallah, D.M. Espino, D.E.T. Shepherd, The barriers to the progression of additive manufacture: perspectives from UK industry, Int. J. Prod. Econ. 198 (2018) 104–118.

[9] L.I. Escano, N.D. Parab, L. Xiong, Q. Guo, C. Zhao, K. Fezzaa, W. Everhart, T. Sun, L. Chen, Revealing particle-scale powder spreading dynamics in powder-bed-based additive manufacturing process by high-speed x-ray imaging, Sci. Rep. 8 (2018) 15079.

[10] W. Nan, M. Pasha, T. Bonakdar, A. Lopez, U. Zafar, S. Nadimi, M. Ghadiri, Jamming during particle spreading in additive manufacturing, Powder Technol. 338 (2018) 253–262.

[11] A. Townsend, N. Senin, L. Blunt, R.K. Leach, J.S. Taylor, Surface texture metrology for metal additive manufacturing: a review, Precis. Eng. 46 (2016) 34–47.

[12] S.A. Khairallah, A.T. Anderson, A. Rubenchik, W.E. King, Laser powder-bed fusion additive manufacturing: physics of complex melt flow and formation mechanisms of pores, spatter, and denudation zones, Acta Mater. 108 (2016) 36–45.

[13] W. Zhang, P. Desai, Machine learning enabled powder spreading process map for metal additive manufacturing (AM), In Int. Solid Free Form Fabr. Symp., Austin, TX 2017, pp. 1235–1249.

[14] A.B. Spierings, M. Voegtlin, T. Bauer, K. Wegener, Powder flowability characterisation methodology for powder-bed-based metal additive manufacturing, Progr. Addit. Manuf. 1 (2016) 9–20.

[15] J. Clayton, Optimising metal powders for additive manufacturing, Metal Powder Rep. 69 (2014) 14–17.

[16] J. Clayton, D. Millington-Smith, B. Armstrong, The application of powder rheology in additive manufacturing, JOM 67 (2015) 544–548.

[17] M. Seifi, A. Salem, J. Beuth, O. Harrysson, J.J. Lewandowski, Overview of materials qualification needs for metal additive manufacturing, JOM 68 (2016) 747–764.

[18] Q.B. Nguyen, M.L.S. Nai, Z. Zhu, C.-N. Sun, J. Wei, W. Zhou, Characteristics of inconel powders for powder-bed additive manufacturing, Engineering 3 (2017) 695–700.

[19] L.C. Ardila, F. Garciandia, J.B. González-Díaz, P. Álvarez, A. Echeverria, M.M. Petite, R. Deffley, J. Ochoa, Effect of IN718 recycled powder reuse on properties of parts manufactured by means of selective laser melting, Phys. Procedia 56 (2014) 99–107.

[20] H.P. Tang, M. Qian, N. Liu, X.Z. Zhang, G.Y. Yang, J. Wang, Effect of powder reuse times on additive manufacturing of ti-6Al-4V by selective electron beam melting, JOM 67 (2015) 555–563.

[21] M. Yan, M.S. Dargusch, T. Ebel, M. Qian, A transmission electron microscopy and three-dimensional atom probe study of the oxygen-induced fine microstructural features in as-sintered ti–6Al–4V and their impacts on ductility, Acta Mater. 68 (2014) 196–206.

[22] A. Strondl, O. Lyckfeldt, H. Brodin, U. Ackelid, Characterization and control of powder properties for additive manufacturing, JOM 67 (2015) 549–554.

[23] G. Egger, P. Gygax, R. Glardon, N. Karapatis, Optimization of Powder Layer Density in Selective Laser Sintering, 1999.

[24] A. Spierings, G. Levy, Comparison of density of stainless steel 316L parts produced with selective laser melting using different powder grades, 20th Annual International Solid Freeform Fabrication Symposium, SFF 2009, 2009.

[25] M. Sadowski, L. Ladani, W. Brindley, J. Romano, Optimizing quality of additively manufactured Inconel 718 using powder bed laser melting process, Addit. Manuf. 11 (2016) 60–70.

[26] Q. Jia, D. Gu, Selective laser melting additive manufacturing of Inconel 718 superalloy parts: densification, microstructure and properties, J. Alloys Compd. 585 (2014) 713–721.

[27] M. Ghadiri, M. Pasha, W. Nan, C. Hare, V. Vivacqua, U. Zafar, S. Nezamabadi, A. López, M. Pasha, S. Nadimi, Cohesive Powder Flow: Trends and Challenges in Characterisation and Analysis, 2020 (KONA Powder and Particle Journal).

[28] Z. Snow, R. Martukanitz, S. Joshi, On the development of powder spreadability metrics and feedstock requirements for powder bed fusion additive manufacturing, Addit. Manuf. 28 (2019) 78–86.

[29] S. Haeri, L. Benedetti, O. Ghita, Effects of particle elongation on the binary coalescence dynamics of powder grains for laser sintering applications, Powder Technol. 363 (2020) 245–255.

[30] J.C. Steuben, A.P. Iliopoulos, J.G. Michopoulos, Discrete element modeling of particle-based additive manufacturing processes, Comput. Methods Appl. Mech. Eng. 305 (2016) 537–561.

[31] S. Haeri, Y. Wang, O. Ghita, J. Sun, Discrete element simulation and experimental study of powder spreading process in additive manufacturing, Powder Technol. 306 (2017) 45–54.

[32] S. Haeri, Optimisation of blade type spreaders for powder bed preparation in additive manufacturing using DEM simulations, Powder Technol. 321 (2017) 94–104.

[33] W. Nan, M. Pasha, M. Ghadiri, Numerical simulation of particle flow and segregation during roller spreading process in additive manufacturing, Powder Technol. 364 (2020) 811–821.

[34] W. Nan, M. Ghadiri, Numerical simulation of powder flow during spreading in additive manufacturing, Powder Technol. 342 (2019) 801–807.

[35] Shop.Buehler. CarbiMEt PSA. [Online]. 2019. [Accessed 16 July 2019]. Available from: https://shop.buehler.com/carbimet-psa-8in-1000p2500.

[36] W.S. Rasband, 2020 Image J. U. S. National Institutes of Health, Bethesda, Maryland, USA, https://imagej.nih.gov/ij/, 1997-2018.

[37] A. Buades, B. Coll, J. Morel, A non-local algorithm for image denoising, IEEE Computer Society Conference on Computer Vision and Pattern Recognition, 2005 , (CVPR'05), 20–25 June 2005 2005. 60–65 vol. 2.